Out-of-Step Protection Based on Discrete Angle Derivatives

Tealane, Marko; Kilter, Jako; Bagleybter, Oleg; Heimisson, Birkir; Popov, Marjan

DOI
10.1109/ACCESS.2022.3193390

Publication date
2022

Document Version
Final published version

Published in
IEEE Access

IEEE Access
Multidisciplinary | Rapid Review | Open Access Journal

Received 5 July 2022, accepted 19 July 2022, date of publication 25 July 2022, date of current version 29 July 2022.

Digital Object Identifier 10.1109/ACCESS.2022.3193390

RESEARCH ARTICLE

Out-of-Step Protection Based on Discrete Angle Derivatives

MARKO TEALANE[1,4], (Student Member, IEEE), JAKO KILTER[1], (Senior Member, IEEE), OLEG BAGLEYBTER[2], (Member, IEEE), BIRKIR HEIMISSON[3], AND MARJAN POPOV[4], (Fellow, IEEE)

[1]Department of Electrical Power Engineering and Mechatronics, Tallinn University of Technology, 19086 Tallinn, Estonia
[2]Grid Automation, GE Renewable Energy, Edinburgh EH10 4QE, U.K.
[3]Landsnet hf., 112 Reykjavík, Iceland
[4]Delft University of Technology, Faculty of EEMCS, 2628 CD Delft, The Netherlands

Corresponding author: Marjan Popov (m.popov@tudelft.nl)

This work was supported in part by the Nederlandse Organisatie voor Wetenschappelijk Onderzoek (NWO) through the Take-Off Project "Power swing detection and prevention in future networks with high penetration of renewable energy," under Grant 19279.

ABSTRACT This paper presents an out-of-step protection algorithm based on angle derivatives, which makes use of wide-area measurements and can be applied on arbitrary tie-lines in electrical power systems. The developed algorithm uses PMU measurements that are taken at both ends of a transmission line. Based on the changes of the electrical quantities in the power system, the algorithm detects unstable system conditions. Thus, the developed solution is settingless and can be easily applied where an out-of-step condition is expected. The concept is deployed by using an industrial controller and tested by conducting numerous hardware-in-the-loop simulations. Additionally, recorded data from actual out-of-step events in the Icelandic power system are used to validate the developed algorithm. The performance of the implemented method is compared against the traditional impedance-based out-of-step protection methods. The results confirm that the proposed algorithm detects out-of-step conditions more reliably and faster than the traditional impedance-based solutions.

INDEX TERMS Out-of-step protection, power system transient stability, tie-lines, real-time HIL testing.

I. INTRODUCTION

Electric power systems are the backbone of modern society. It is very important that the power system remains operational at all times. The continuous increase of energy demand puts additional stress on the power network, and forces the system to operate closer to the stability limits. In addition, the growing amount of renewable energy sources increases the intermittency of the power generation accordingly, putting additional stress to the power system. Moreover, disturbances like short-circuit faults naturally occur during power system operation. As the system becomes more stressed, a variety of disturbances can propagate into a larger scale event, causing a major imbalance between the mechanical input and the electrical output power of the generators, resulting in a loss of synchronism in the power system. This is known as an out-of-step (OOS) condition and it causes additional mechanical and thermal stresses on power system components, which can lead to catastrophic failure of equipment and blackouts in the electrical power system [1]. Therefore, protection systems must be ready to detect and react to this kind of conditions in order to prevent permanent failure of crucial equipment and avoid blackouts.

The conventional OOS protection is realized by impedance relays and is based on the trajectory of the impedance, the rate of change of the impedance and the continuity of the computed impedance value [2]. Impedance-based methods are easy to implement, however, to operate correctly, they need specific settings. Therefore, they are susceptible to challenges because of network reconfigurations, and the computation of settings is time consuming due to required extensive system stability studies.

The associate editor coordinating the review of this manuscript and approving it for publication was Sarasij Das.

TABLE 1. Existing OOS protection methods and approaches in literature and industry.

Classification	Method	Advantages	Limitations
Commercially available OOS detection approaches	Impedance-based detection [1] [2]	Depending on the implementation, can differentiate between stable and unstable swings.	Difficulties in detecting very fast swings; rigorous analysis is required to set the blinders; no predictive properties
	Angle-controlled OOS protection [3]	More reliable and faster than impedance-based OOS protection	Needs predetermined settings to operate and cannot adapt to system reconfigurations; no predictive properties.
	R-Rdot method [4]	Faster detection compared to impedance-based detection	Requires protection settings; no predictive properties.
	Superimposed current detection [5]	Very fast swing detection, ability to detect fast swings.	Difficulties in detecting slow swings, no discrimination between a stable and unstable swing; no predictive properties.
Unconventional OOS detection approaches based on local measurements	Detection based on Power-time (*P-t*) curve [6] [7]	Instability is directly detected from measurements.	Can only be applied directly at generator terminals; no predictive properties.
	Faster than real-time OOS detection [8]	Provides extremely fast OOS detection; predicts if a swing will become unstable.	Requires detailed knowledge about generator parameters; can only be applied directly at generator terminals.
	Lyapunov function based OOS detection [9]	The method shows excellent results in OOS detection.	Highly dependent on the estimation of swing-center voltage value.
Unconventional OOS detection based on wide-area information	Direct angle comparison based OOS protection [10]	The method does not require any computation of protection settings.	Requires monitoring of all the generator buses in the network; operates after several out-of-step cycles.
	Predictive OOS based on synchrophasors [11]	Enhances existing OOS protection, provides more secure and reliable operation for oscillatory OOS compared to existing methods; has predictive properties.	OOS detection speed is not known; not effective in detecting non-oscillatory unstable swings.
	Clarke transform based method [12]	Provides settingless OOS protection, has been prototyped in a real industrial system.	OOS detection speed is not elaborated; no predictive properties.
	Machine learning approaches [13] [14] [15]	Methods offer fast and accurate OOS condition detection, can predict OOS conditions.	The correct performance of the methods requires extensive training using detailed models.
	Proposed approach	Method *does not* require offline studies or predetermined settings. It *provides* faster and more reliable OOS detection than conventional approaches, and has been fully prototyped.	No predictive properties.
	OOS detection based on PMU-determined impedances [16]	The method is more secure and provides faster OOS detection than conventional solutions.	Requires a step change in the network to determine network impedances for OOS detection; no predictive properties.
	Fast online coherency OOS detection [17]	The method shows more reliable OOS detection than conventional solutions.	OOS detection speed is not elaborated; only applicable at generator terminals, requires a threshold setting; no predictive properties.
	Voltage fluctuations based OOS detection [18]	The method shows fast detection of instability.	Requires a high level of observability in the network; no predictive properties.

Table 1 represents an overview of currently available approaches to detect an OOS condition, based on the prior industrial and academic achievements. The advantages and the limitations of the conventional and notable non-conventional OOS protection methods that have been published so far are highlighted.

In [3], an angle-controlled OOS protection is proposed, in which the whole power system is reduced to a two-terminal network, and the equivalent generator voltage vectors are compared. This also relies on the predetermined impedance settings of the equivalent networks, and thus is difficult to adapt to real-time system reconfigurations. The solution proposed in [6] utilizes power-time curves at the measured location to determine generator stability by applying the energy equilibrium criterion. The advantage of this approach is that the instability is detected directly from the power-time

$(P-t)$ curve, and it does not require any network reduction and offline studies. However, this concept can be applied only directly at the generator terminals and not on tie-lines in the network because in a multi-machine network, each generator output needs to be individually monitored. In [8], the authors proposed a method to detect the generator instability by utilizing measurement data during the disturbance. With this method, the simulations are run faster than the measurements in real-time. This solution results in a very fast OOS detection, however, it requires detailed knowledge about the generator parameters, which a network operator might not have access to.

Additionally, there are also approaches that have made use of machine learning techniques to tackle the OOS problem [13]–[15]. These approaches, however, require extensive model simulations for the purposes of training the machine learning algorithms, and therefore do not show major advantages (at present) over the classical impedance-based protections.

Furthermore, a number of effective OOS protection methods based on wide-area information have been published recently in literature. Some of the most notable recent work can be found in [19]–[21] and [22]. All these methods, however, rely on measurements that are located directly at the generator terminals or at the corresponding high-voltage terminals. This limiting factor is often overlooked, while it makes the developed methods difficult to apply in actual power systems due to the lack of coverage of PMUs in a large power system.

Apart from the methods listed in the comparative table, some recent work on OOS protection based on local measurements include [23], [24] and [25]. These methods, however, can only be applied on generator terminals, since they require direct input from generator measurements.

In addition there exist OOS protection algorithms in literature, that make use of state estimation techniques together with local and wide-area information in [26]. The method shows improved results compared to impedance-based generator OOS protection, however, the effectiveness of this method on arbitrary tie-lines in the network has not been investigated.

This paper proposes a new OOS protection algorithm based on angle derivatives, which requires only two PMU measurements to be applied. The developed algorithm is suitable to be used in arbitrary power systems on transmission lines where an OOS condition can be expected. It relies on PMU measurement data from both ends of the transmission line, and is based on the well-known power-angle curve, and the stability phenomena of the power system when an OOS condition takes place. The novel algorithm is implemented and tested using an industrial controller by using real-time hardware-in-the-loop (HiL) simulations. A real-time simulation model of the Icelandic power system (Landsnet) is developed and validated using measured OOS event data. This model, as well as the existing wide-area measurement data from Landsnet, are used for testing the proposed algorithm in various scenarios. Furthermore, a comparative study using two commercially available impedance-based OOS relays and the newly developed solution is performed in a customized IEEE 39-bus network.

The rest of the paper is organized as follows: Section II presents the proposed algorithm; Section III describes the methodology for the algorithm testing; Section IV details and validates the real-time network model of the Icelandic power system; Section V shows the performed case studies with results, and finally, the paper ends up with conclusions.

II. PROPOSED ALGORITHM

A. THE OUT-OF-STEP PHENOMENON BACKGROUND

The proposed algorithm relies on the widely applied power-angle characteristic of a generator. According to the classical representation, a generator's dynamic behavior is represented by the swing equation [27] (1) as follows,

$$\frac{M}{\omega_s}\frac{d^2\delta}{dt^2} = P_m - P_e(\delta) \tag{1}$$

where M - the inertia constant of the equivalent machine; ω_s - the rotor speed of the generator; δ - the internal voltage angle of the generator; P_m - the mechanical input power of the generator; P_e - the electrical output power of the generator.

The electrical output of the generator ($P_e(\delta)$) depends on the angular difference of two equivalent voltage phasors that are separated by impedance x_{tot}. This relation forms, what is known as, the power-angle curve of a generator and is expressed by equation (2),

$$P_e(\delta) = \frac{|\overline{E}_1||\overline{E}_2|}{x_{tot}}\sin\delta \tag{2}$$

where $|\overline{E}_1|$, $|\overline{E}_2|$ - the equivalent internal voltage phasor magnitudes of the sources; x_{tot} - the equivalent reactance between the two sources, and δ - the angle difference of the equivalent phasors.

The resistances of machines and transmission lines are neglected in equation (2), since resistances introduce a damping term in the swing equation. In addition the mechanical input power of the generators is assumed to be constant, as well as the generators are assumed to be constant voltage sources behind a reactance, which neglects the effects of automatic voltage regulation. In this way we consider the worst-case scenario of the power-angle relationship in the network. Furthermore, it should be acknowledged that the due to the these reasons the actual power-angle curve may deviate from the idealistic curve, which is used to explain the general phenomenon of transient stability. However, it has to be pointed out, that in the networks used for case studies, the generators are equipped with voltage control and the resistances are considered as well as the losses in the network. With this approach the algorithm is tested in near-realistic conditions.

This power-angle curve can be applied to determine the power transfer across a single transmission line in a meshed

transmission network. A multi-machine system can be separated into two groups of machines, that represent the inertia centers at either end of a transmission line [28]. Note that the equation (2) is applicable also for power flow through an arbitrary transmission line, when the equivalent internal voltage phasors are replaced with the voltage values at the ends of the transmission line in question. Hence, by using the power-angle curve, the dynamic stability around a tie-line can be assessed.

Fig. 1b represents the power-angle characteristics for pre-, faulted- and postfault state of a two-machine equivalent system shown in Fig. 1a. On the power-angle characteristic, two operating points can be determined by using a prefault steady-state power transfer (noted as P_m). The operating point located in the left half of the characteristic is a stable operating point. According to the Equal Area Criterion (*EAC*) [27], the maximum angle difference of a recoverable swing cannot be greater than the second operating point (called Last Stable Angle - *LSA*), though it may be smaller. The further increase of the angle difference beyond the *LSA* point will definitively result in an unstable generator operation. Thus, the *LSA* point is critical to distinguish between a stable and an unstable swing. The *LSA* point is located on the postfault curve, which sits lower than the prefault curve due to the transmission impedance increasing upon switching off the faulty element.

When observing the dynamic behavior of a power system, it can be noted that during a fault, the electrical active power is lowered due to the reduced voltage magnitudes. However, the mechanical energy given to the generators by the prime movers remains rather constant. Due to this difference in energy the angular difference between the equivalent voltages begins to increase. After the fault clearing the increased value is indicated as δ_1, and the surplus of energy obtained during a fault condition is indicated by the shaded area in Fig. 1b.

Thereafter, the electrical output power is higher than the mechanical input power, and the increase of the angular difference is slowing down. Due to inertia, the angular difference keeps increasing, until the surplus of energy obtained during fault disappears. This means that during that time the first derivative of the angle value will be positive, because the angle difference keeps increasing. However, the second derivative of the angle difference will be negative, since the rate at which the angle is increasing, is lowering. In addition, during this process the electrical power output will also be increasing. Accordingly, the first derivative value of the active power will have a positive value. The angular difference will increase until reaching a maximum value denoted by δ_m. At this point, equality between the obtained and the dissipated energy is reached. This process is illustrated in Fig 1c.

Once the maximum angle value is reached, the angular difference will start to decrease, and the system will move towards a new stable equilibrium point. During this process, the angle change speed and the change in active power will be negative, thus the derivative values are negative. The process is illustrated in Fig. 1d, and is known as a stable power swing. It has to be noted that during a stable power swing

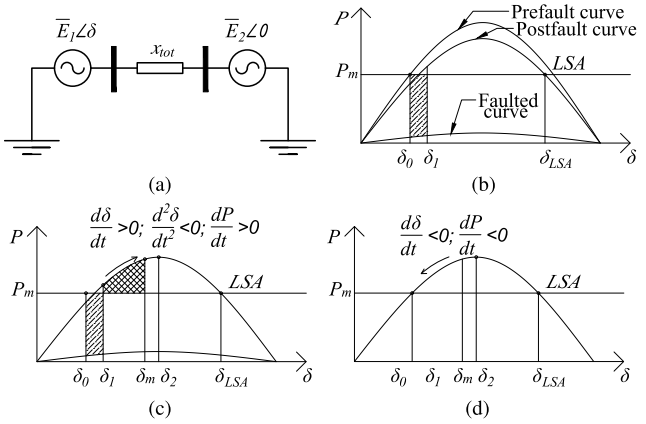

FIGURE 1. Two-machine system and the demonstration of a stable power swing process on a power-angle curve. (a) Two-machine equivalent with a connecting transmission reactance, (b) Power-angle curve illustrating the pre-, faulted- and postfault operations, with the Last Stable Angle point denoted as δ_{LSA}. (c) Power system operation after a disturbance; during this operation the angle difference is decelerating until reaching the maximum angular difference of δ_m, where the surplus of energy has all been dissipated. (d) Power system operation after the surplus of energy after the disturbance has been dissipated and the angular difference is decreasing while system is settling at a stable operation point.

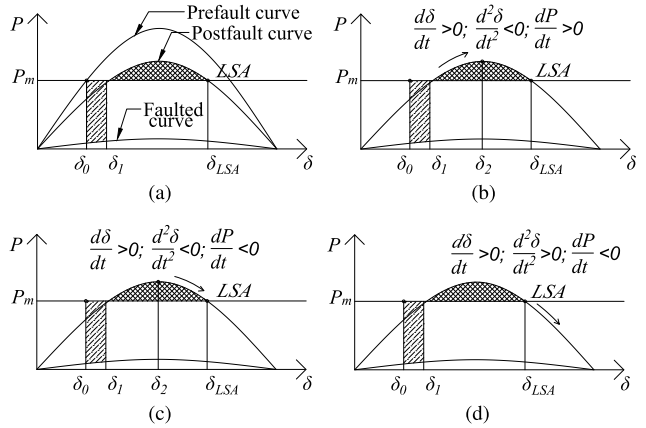

FIGURE 2. Demonstration of an unstable power swing process on a power-angle curve (a) Power-angle curve illustrating the pre-, faulted- and postfault operations, with the Last Stable Angle point denoted as δ_{LSA}. (b) Power system operation after a disturbance, during this operation the angle difference is decelerating, and power derivative remains positive until reaching the maximum active power value at δ_2. (c) Power system operation after passing the maximum power value, during this operation the power derivative is negative and the angle difference is decelerating until reaching the Last Stable Angle point. (d) System operation becomes unstable after passing the Last Stable Angle point.

the operating point may pass beyond the maximum power point δ_2, however, it will not cross δ_{LSA}.

The process of an unstable swing is illustrated in Fig. 2, where post-fault impedance is assumed to be higher than in the stable case. For comparison purposes this example of an unstable swing is again started with a fault in the power system. The beginning of the swing process is similar to the stable swing explained before, and is illustrated in Fig. 2a. After the fault clearance the angular difference

is again increasing, and during the start of the process the acceleration and the speed of the angle change have the same signs as those with the stable swing, as illustrated in Fig. 2b. However, in this case, the angular difference continues to increase, passing the point δ_2 in the power-angle curve. The electrical power value begins to lower, and consequently the derivative of power will become negative, as illustrated in Fig. 2c. Subsequently, with the further increase in angular difference, the *LSA* point (denoted by δ_{LSA}) will be passed. When the system has passed this point, the angular difference will start accelerating. This means that the stable operation of the power system is no longer possible and the system will experience an OOS condition. This condition is indicated by the second derivative of the angle value becoming positive, with the first derivative value remaining positive. Simultaneously, the first derivative value of the active power is negative. This situation is illustrated in Fig. 2d. It has been shown that the use of the power-angle characteristic and *EAC* concept applies for assessing complex stability phenomena in large multi-machine systems, in addition to a two-machine equivalent network [29].

It should be noted, however, that in reality the power-angle curve is different than the idealised curve used for the explanation above, i.e. the amplitude value of the power-angle curve is shifted away from the theoretical maximum at 90 degrees. The reason for this is that the voltages are not constant and the losses are not taken into account. The mechanisms and mathematical explanation of the variations in the power-angle curve are discussed in more detail in [30] and [31].

To summarize, the growing angle difference and dropping active power together point to the right half of the power-angle curve, while the change of sign of the angle difference acceleration (second derivative becoming positive) indicates the crossing of the *LSA* point. These three criteria unambiguously identify that the power swing becomes non-recoverable and therefore can be used as a basis for the proposed OOS protection algorithm.

B. DEVELOPED OUT-OF-STEP PROTECTION ALGORITHM

The developed protection algorithm uses the measurements provided by the PMUs on both ends of a transmission line. This allows for the computation of angular difference derivative values, in addition to the monitoring of the voltage, current and power values.

It must be noted that due to the discrete nature of PMU measurements the continuous derivatives mentioned in Section II should be substituted with finite differences, i.e. we are supposed to replace $\frac{d\delta}{dt}$ with $\frac{\Delta\delta}{\Delta t}$. Nevertheless, for the purpose of simplicity we will continue to use the same terminology as above, bearing in mind that all the derivatives will be estimated using sampled discrete measurements and finite differences.

According to the explanation given above for an OOS condition, shown in Fig. 2d, the criteria for the protection operation are as follows:

$$\begin{cases} \dfrac{d\delta}{dt} > 0 & \text{for two consecutive measurements} \\ \dfrac{d^2\delta}{dt^2} > 0 & \text{for three consecutive measurements} \end{cases}$$

These conditions might be also fulfilled during normal operation, while the operating point is situated in the stable operation area of the power-angle curve. In order to stop the OOS protection algorithm from operation during normal conditions, blocking and restraining criteria have been defined. The criteria for *blocking* the protection function during normal grid conditions are as follows:

$$\begin{cases} \text{Measured voltage above 0.89 p.u.} \\ \text{Measured voltage below 0.2 p.u.} \end{cases}$$

The first criterion is used to ensure protection is blocked when the network operates in nominal condition. The second criterion is used to check if there is a fault present on the protected line. The values proposed above should be considered as indicative, the exact thresholds may be adjusted based on the local deployment conditions. If either of those conditions are fulfilled, the protection will not operate.

In order to *restrain* the protection from operation while the system is experiencing a stable power swing, the following criteria are used:

$$\begin{cases} \dfrac{dP}{dt} > 0 & \text{for two consecutive measurements} \\ \dfrac{dV}{dt} > 0 & \text{for two consecutive measurements} \end{cases}$$

The first criterion restrains the protection from operating whilst the operation point is located in the first half of the power-angle curve, where, during the angular difference increase, the active power transfer also increases. The second criterion restrains the protection algorithm from operation when the system is in the process of leaving the swinging condition, and the voltages increase. The objective of using these criterion is to allow the protection to only operate when the system is moving towards instability after passing the theoretical maximum power transfer point on the power-angle curve.

It has to be noted that the algorithm requires multiple consecutive measurements to fulfill the presented criteria in order to operate, in order to avoid the algorithm from operating from a singular measurement result which may be caused by noise. Therefore, the operation time of the algorithm is also dependent on the sampling rate used for the input data streams.

The algorithm is divided into three main segments and its structure is shown in Fig. 3. The first segment, circled in red in Fig. 3, is responsible for checking the data validity and blocking the protection based on voltage measurements. The second segment, circled in green, computes and assesses the active power and voltage derivative values and restrains the protection operation if necessary. Finally, the

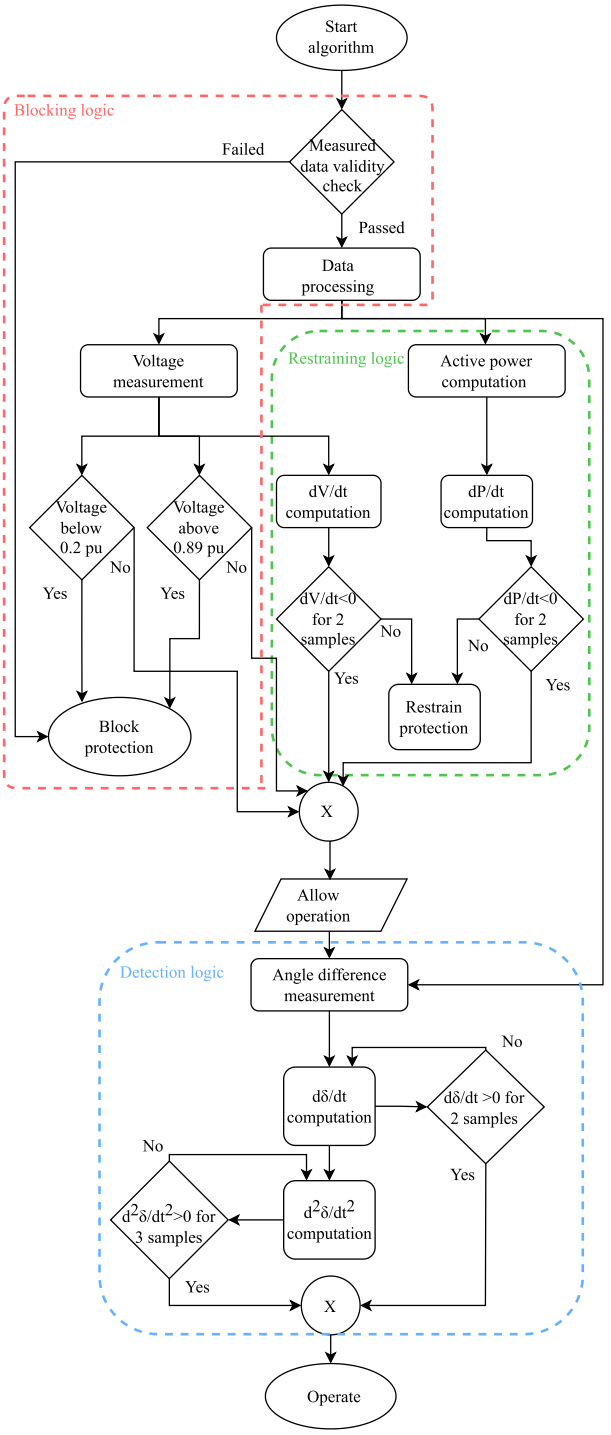

FIGURE 3. Principle diagram of the developed OOS protection algorithm.

third segment, denoted in blue, computes the first and second derivatives of the angle difference, and is responsible for OOS detection and protection operation command. The main advantages of the developed algorithm compared to existing solutions are, that it requires no offline studies or simulations and requires little processing power, therefore it is easily adoptable on already existing hardware.

III. TESTING METHODOLOGY AND TEST SETUP

In this section, the implementation of the developed algorithm is explained together with the simulaion platform and the IEEE 39 bus model used as a testing network. The algorithm is tested using HiL simulations by feeding PMU measurement data into a dedicated phasor-based controller. Simultaneously, analogue voltage and current waveform signals are provided to the impedance-based OOS protection devices in order to compare the performance of the new method and existing solutions.

A. IMPLEMENTATION OF THE DEVELOPED ALGORITHM FOR HiL TESTING

The algorithm is developed and deployed on an external programmable controller device [32]. This phasor-based controller is capable of receiving multiple PMU data inputs and executing complex custom-built algorithms in a fast, deterministic manner.

The data validity check shown at the start of the algorithm in Fig. 3 is handled by the controller hardware. If the measured data does not pass the validity check, meaning that the data is not time-synchronized or PMU frames are missing, the protection algorithm is blocked. When the validity check is passed, the measurement values are allowed to be supplied to the protection algorithm described in Section II.

The controller, where the proposed algorithm is implemented, receives measurement data from real-time simulations over an Ethernet network according to IEEE C37.118 standard. The data rate used affects the decision time of the algorithm, since the algorithm's criteria are linked to consecutive measurements. Therefore, the slower the data rate, the slower the decision time. For uniformity throughout the paper, the PMU data rate used for the tests conducted with IEEE 39 bus networks was 60 fps (frames per second). The data rate for tests with the Icelandic simulated network, as well as recorded OOS events from Iceland, was 50 fps. The controller provides feedback signals and calculated values back to the Real-Time Digital Simulator using IEC 61850 GOOSE messages. PDC (Phasor Data Concentrator) Wait Time [33] of 100 ms was implemented in the controller in order to consider the representative latency of the data collection using PMUs from different geographic locations. The processing cycle time of the controller was configured at 16.667 ms and 20 ms for the IEEE 39 bus network and Icelandic system tests respectively.

The proposed algorithm installed on the controller is tested in parallel with two physical relays using HiL test setup. The illustration of the setup is shown in Fig. 4. The information marked by red represents the input values to the hardware: analogue voltage and current signals for the impedance-based OOS protection relays, and IEEE C37.118 PMU data for the phasor-based controller. The information marked in green shows operation signals in the form of digital inputs from the relays and IEC 61850 data for the controller. The particular test scenarios and the test network model are explained further in the next sections.

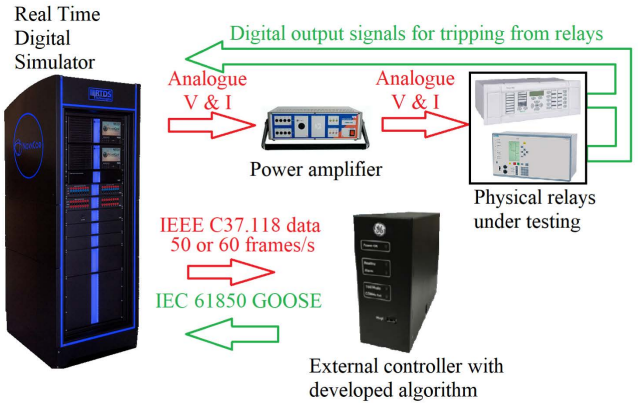

FIGURE 4. Experimental setup for HiL OOS protection testing using hardware.

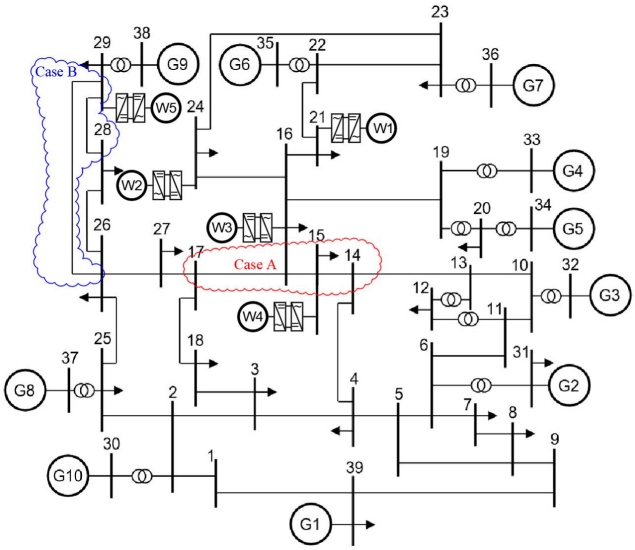

FIGURE 5. Modified IEEE 39 bus network with added type 4 wind farms. Red marks Case A testing location and blue Case B testing location, wind farms W1-W5 are added to buses 21, 15, 25, 16 and 29, respectively.

B. MODIFIED IEEE 39 BUS TEST SYSTEM AND TEST CASES

In order to test the performance of the algorithm in a multi-machine network, the IEEE 39 bus network model was used. The model is modified by adding generic grid-following wind farms (W1 - W5) at some buses, using an existing wind power plant model in the simulation software [34]. In this way, the developed solution can be tested for different grid and generation mix conditions. The modified test network is shown in Fig. 5. Two different test locations are chosen to investigate different power swing conditions in the network and test the protection devices for various scenarios. The first test location is circled in red and shown as Case A, whilst the second denoted in blue is Case B. The former location demonstrates the power swing scenario occurring between two larger parts of the network, while the latter location represents a case of a single machine connected to an infinite bus system.

Both locations cover two tie-lines each in order to see the proposed algorithm's behavior for different tie-line lengths. For Case A, the protection was tested for the lines between buses 14-15 and 16-17. To create an OOS condition in the power system, a three-phase short circuit is applied on bus 16. The fault is cleared by disconnecting one of the transmission lines emanating from bus 16, and thereafter power swings take place on the remaining tie-line between the two parts of the network. For Case B, the transmission lines under observation are those between buses 26-29 and 28-29. Power swings are created by applying a three-phase short circuit on bus 29. The fault is cleared by disconnecting one of the two tie-lines connected to this bus, leading to power swings along the remaining transmission lines.

For the studied Case A, the impedance-based protection relays are situated on bus 15 for line 14-15 and on bus 16 for line 16-17. For Case B, the impedance-based protection relays are at bus 29 of the transmission lines for both tested lines. The PMUs that stream measurement data to the phasor-based controller are situated on both ends of the transmission lines in all of the tested cases.

Both of the tested relays incorporate an impedance-based OOS algorithm, and are set to trip on the way in (TOWI) and on the way out (TOWO) of the configured impedance characteristic. The settings of the protection devices are obtained according to the manufacturer guidelines as explained in the user manuals of the relays; the settings were calculated using a base case of fully synchronous system [35], [36].

In order to test the OOS protections for various grid conditions, the output power of the wind power plants is scaled up while simultaneously decreasing the synchronous generation capacity. For Case A, for a specific renewable penetration scenario (RES %), all four wind power plants (denoted as W1-W4 in Fig. 5) in the network area provide the specific percentage of the base case synchronous generation output of the four generators (denoted as G4, G5, G6 and G7) in the area. At the same time, the apparent power of these generators is decreased from the initial value of 1000 MVA by the same specific percentage of the RES % level. This is done in order to also decrease the total inertia of the generators together with their output power. For Case B, one generator (G9) and one windfarm (W5) are scaled accordingly. Additionally, at each RES % case the simulation is repeated five times to evaluate the consistency of the tested OOS protection devices. This results in a total number of 300 real-time simulations for the case studies using IEEE 39 bus test network.

C. CONCEPT VERIFICATION

In this subsection, the developed algorithm's response to a stable and unstable swing for Case A location in the IEEE 39 bus network is shown.

The case of a stable power swing is shown in Fig. 6. The swing is initiated by a five-cycle long fault in the system occurring at 0.15 seconds (shown by ①), after which the system goes through a stable swing. Fig. 6a shows the signals associated with the developed algorithm in the controller,

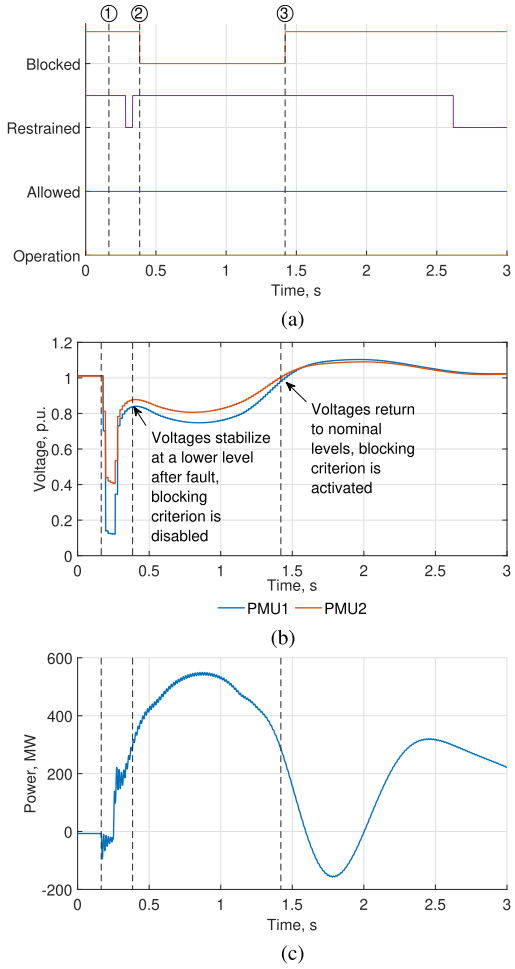

FIGURE 6. Protection algorithm response signals, voltages at both ends of the transmission line and active power through the line during a stable power swing in the network. (a) protection algorithm signals in the external controller, (b) the voltage magnitudes at both ends of the protected transmission line and (c) the active power through the protected line.

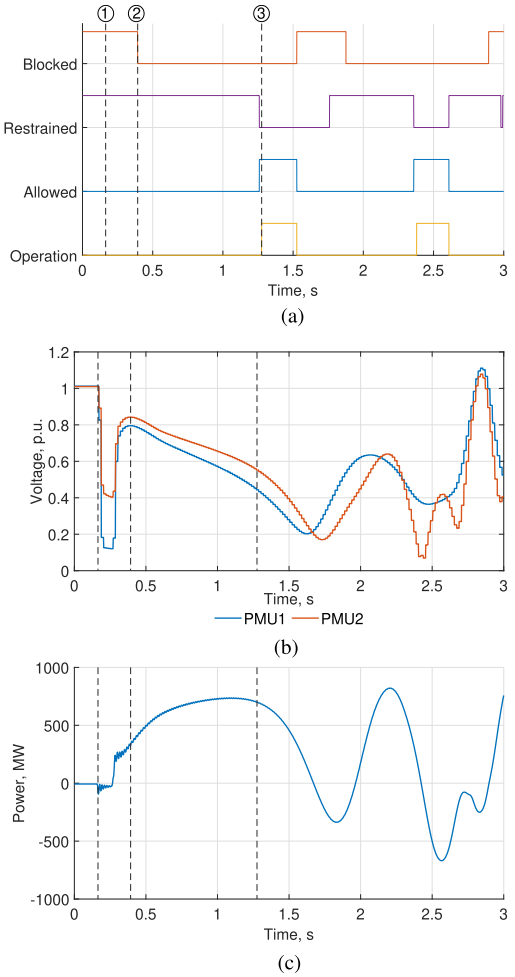

FIGURE 7. Protection algorithm response signals, voltages at both ends of the transmission line and active power through the line during an unstable power swing and subsequent OOS condition. (a) protection algorithm signals in the external controller, (b) the voltage magnitudes at both ends of the protected transmission line and (c) the active power through the protected line.

as described in Section II of this paper. Figs. 6b and 6c illustrate the streamed measurement values of the voltage and the active power through the transmission line from the real-time simulation. It can be observed that after the short-circuit condition has ended, the blocking criteria for the protection function are disabled (specified by ②). However, the restraining criteria are inactive only for a very short duration, right after the fault has been cleared, and, thereafter become active, because the power transferred through the transmission line is increasing, thus the derivative value is positive. In addition, once the power starts decreasing, the voltage value starts increasing. Due to this behavior, the restraint criterion remains active and the protection provides no operation command during a stable swing. After some time the voltage values return to nominal operation level and the blocking criterion is activated, as indicated by ③.

The reaction of the algorithm to an unstable power swing is shown in Fig. 7. The swing is initiated by a six-cycle fault in the system occurring at 0.15 seconds (shown by ①), after which the system experiences an unstable swing. Fig. 7a shows the developed algorithm signals in the controller, whilst Figs. 7b and 7c show the measured quantities from the simulation. From the response of the protection, it can be observed that after the short-circuit fault the blocking criterion is disabled, as shown by ②. This is because the voltage value is out of bounds of the blocking criterion. However, the restraint criterion is active, since the measured active power transfer through the transmission line is increasing. In the meantime, it can be seen that the voltage value is decreasing, and, accordingly, the derivative of the voltage value is negative. Once the active power starts decreasing, the restraining criterion deactivates. This means that both the blocking and the restraining criteria are not active; therefore the protection will issue an operating command as soon as the first and second derivatives of the angular difference are both positive for two and three consecutive consecutive cycles respectively. The protection detects the unstable condition, which is seen

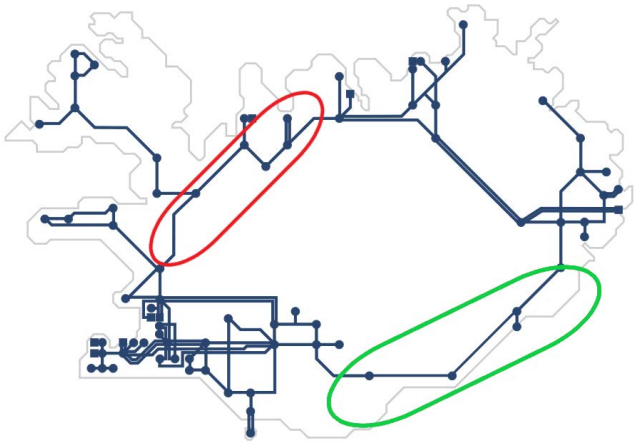

FIGURE 8. Icelandic power system, the corresponding corridors of lines connecting two parts of the network are outlined in red and green for the northern and southern ring connections respectively. [37].

by the operation signal activation at instance ③. Hence it can be concluded that the developed protection algorithm is able to distinguish between unstable and stable swings in the network, and is able to issue tripping commands when there is an unstable power swing developing on the protected line.

IV. ICELANDIC POWER SYSTEM MODEL VERIFICATION FOR REAL-TIME SIMULATIONS

To display the developed algorithm's robustness for the application in arbitrary power systems, the Icelandic power system has been used for additional simulations. In order to perform real-time simulations to test the OOS protection, the Icelandic power system was modelled in RTDS environment. Fig. 8 shows the Icelandic power system, which has two centers of inertia, situated in southwest and in the eastern part of the island. The two main centers of inertia are connected with links, known as the northern ring connection (north corridor), circled with red, and the southern ring connection (south corridor), circled with green. In addition, the southern ring connection uses series compensation by utilizing a series capacitor that can be switched on or off. On these two ring connections power swings are expected, and the developed protection algorithm is expected to be installed.

The Icelandic grid uses a wide-area monitoring system with a number of PMUs installed in the network. The wide-area monitoring system has recorded several system-level events including OOS conditions, which are used to compare the developed network model behavior to the actual system behavior. The network model in RTDS environment was developed based on the PSS/E® network model provided by Landsnet.

Two recorded OOS events were used to validate the created model in RTDS. The first OOS event was initiated by a busbar flashover in one of the substations located in the northern ring connection, which led to the loss of the substation and disconnection of the northern transmission corridor, resulting

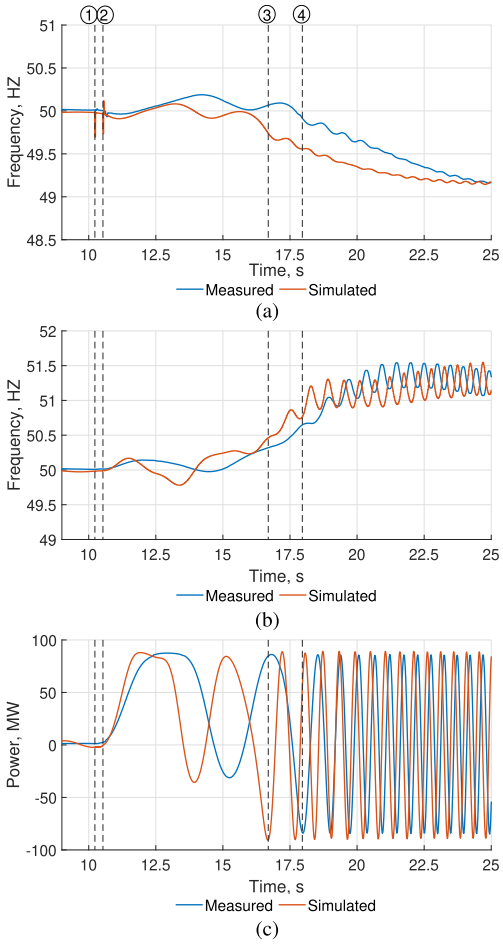

FIGURE 9. OOS event 1 measured and simulation values. (a) the frequency in the south-west center of inertia, (b) the frequency of the east center of inertia and (c) the active power flow in the southern ring connection, where the OOS event takes place. ① - the start of the event with the fault in the north corridor substation, ② - fault clearance, ③ - first pole slip in simulated values, ④ - first pole slip in measured values.

in an OOS condition in the southern ring. The second event was initiated by a sudden loss of load in the south-western inertia center. This contingency caused system split, where some generators in the south west system were connected to the rest of eastern network only through the southern ring connection, and led to an OOS condition in the southern corridor of the network.

The comparison of the measured values and the simulated results for the first OOS event is shown in Fig. 9. The frequencies of the south-western inertia center and the northern inertia center are shown in Figs. 9a and 9b, whereas the active power flow in the southern corridor during the event is shown in Fig. 9c. The specific events of interest are marked throughout the subfigures, where ① marks the start of the sequence of events with a flashover at the substation in the northern corridor, at 10.2 seconds. After 300 ms (marked as ②), the fault is cleared by tripping the remote ends of the lines from the faulted busbar, leading to the disconnection of the northern transmission corridor. Thereafter, the active

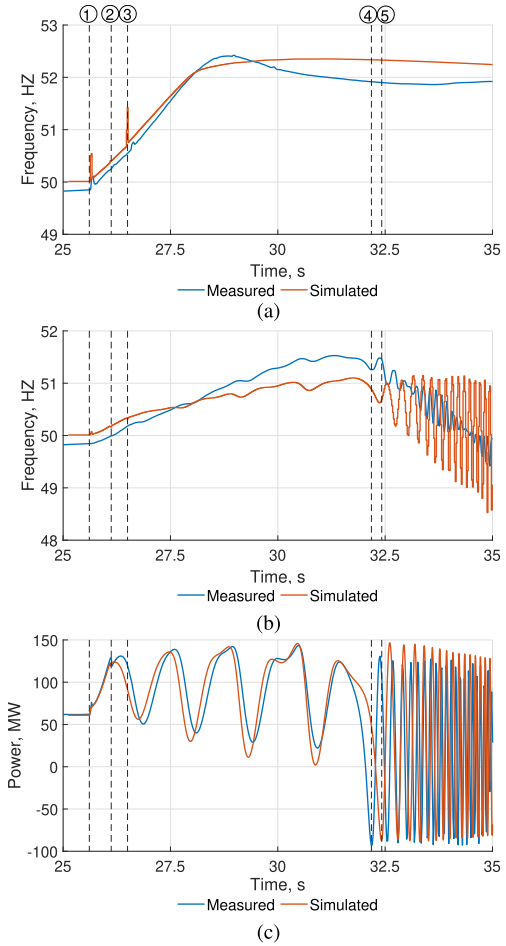

FIGURE 10. OOS event 2 measured and simulation values. (a) the frequency in the south-west center of inertia, (b) the frequency of the east center of inertia and (c) the active power flow in the southern corridor, where the OOS event takes place. ① - the start of the event with the loss of load, ② - inter trip on the 220 kV substation at the southern corridor, ③ - north corridor disconnection from overload, ④ - first pole slip in measured values, ⑤ - first pole slip in simulation.

power is transferred through the southern corridor, and the system goes through a stable swing, after which it fails to maintain stability. The northern and southern parts of the network experience the first pole slip at ③ and ④ for the measured and simulated results respectively.

It can be observed that the simulated and measured data show a slight deviation, however, the general behavior of the simulated network and the measurement data is similar. For both cases, after the initial event occurs, the system goes through a stable swing. The simulated results show greater swing frequency than the measured one. This is likely caused by a difference in generator dispatch during the event, as well as by the effects of the user-defined governor models.

The comparison of the measured values and simulated results for the second OOS event is shown in Fig. 10. The frequencies of the south-western inertia center and the northern inertia center are shown in Fig. 10a and Fig. 10b, respectively, whereas the active power flow in the southern corridor during the event is shown in Fig. 10c. The specific events of interest are marked throughout the subfigures, where ① denotes the start of the sequence of events with a large loss of load in the network at 25.6 seconds. The loss of load is followed by an inter-trip from the overload protection of the southern corridor marked as ②. Due to disconnection in the 220 kV substation nearest to the southern link, only two generators remain connected to the network through the southern corridor. At ③, the northern corridor link is disconnected by the overload protection, effectively separating the two inertia centers of the network. As a result, the two generators left on the southern corridor pass through three stable power swings, which are increasing in magnitude, and experience a pole slip at ④ and ⑤ for the measured values and simulation results, respectively.

From the comparison of the measured and simulated values it can be observed that the simulated results are well aligned with the actual measured values for this event. The frequency in the south-western inertia center follows closely the measured values, and in the northern part there is a slight difference in the gradient of the frequency increase, which may be caused by a difference in production units during the actual event and the simulation, together with the effect of non-standard governors used in the Icelandic power system. As for the power flow in the southern corridor, the simulated values closely match the measured values. Based on these results, it can be concluded that the model follows the real-life characteristics of the Icelandic power system and can be used to investigate OOS protection algorithm in the future.

V. CASE STUDIES

This section presents the test results of the developed protection algorithm using real-time simulations with the IEEE 39 bus test network and the recorded data from OOS events in the Icelandic power system, as well as the simulations with the developed Icelandic power network model. While there are numerous other methods developed for OOS protection, as shown in Section I, the aim of the conducted case studies is to compare the performance of the developed solution to currently available impedance-based protection devices.

A. COMPARATIVE RESULTS FROM IEEE 39 BUS NETWORK SIMULATIONS

In this subsection, the results of the comparative analyses of the developed algorithm and the currently available impedance-based OOS protection relays are shown. The overall detection rate of the OOS conditions for both of the test cases, and the tested algorithms, is shown in Fig. 11.

Regarding Case A, it can be seen that Relays 1 and 2 fail to operate in 6.7 % and 3.6 % of all the performed tests respectively. In contrast the new algorithm operates in 100 % of all the tests. However, when looking at a single machine going OOS with the rest of the system (Case B), the conventional relays show significantly lower detection rates compared to the developed algorithm. The failure rate is 23 % and 22.2 % for Relay 1 and Relay 2, respectively. At the same time, the

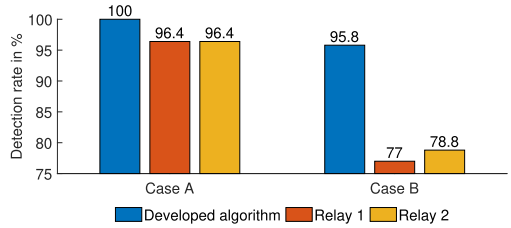

FIGURE 11. OOS condition detection rates for developed algorithm and tested relays in percentage across the simulated cases A and B.

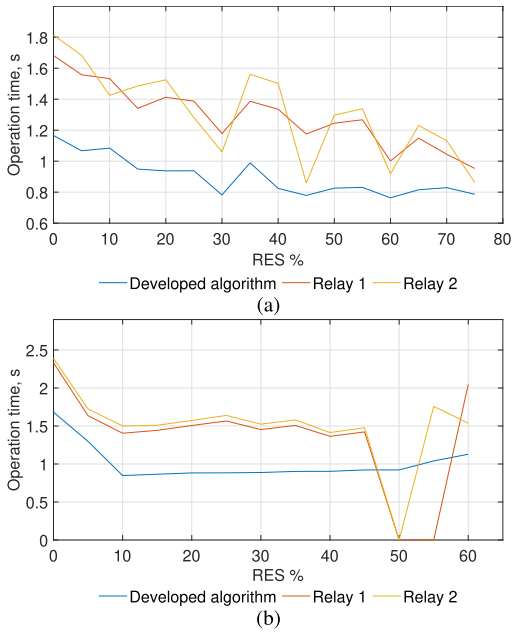

FIGURE 12. OOS protection operating times of protection devices for Case A. (a) represents a case study on the transmission line between buses 14-15 and (b) represents a case study on the transmission line between buses 16-17.

developed algorithm successfully operates in 95.8 % of the Case B tests, giving the failure rate of 4.2 %.

1) COMPARISON OF RESULTS IN CASE A

The operating time comparison between the two tested impedance-based relays and the developed OOS algorithm is shown in Fig. 12. The operating times show how long it takes the protection device to provide a trip command after the short-circuit fault has been cleared. The value of '0' means that the protection device did not provide any tripping command within five seconds after the OOS condition, at which point the simulation is terminated. Fig. 12a shows the operating times when the protection is installed on the transmission line between buses 14-15, and Fig. 12b shows the operating times when the protection is used on the transmission line between buses 16-17.

From this figure it can be observed that the developed algorithm shows significantly lower operating times on both of the installed transmission lines. The developed algorithm, on average, is 490 ms and 540 ms faster compared to Relay 1

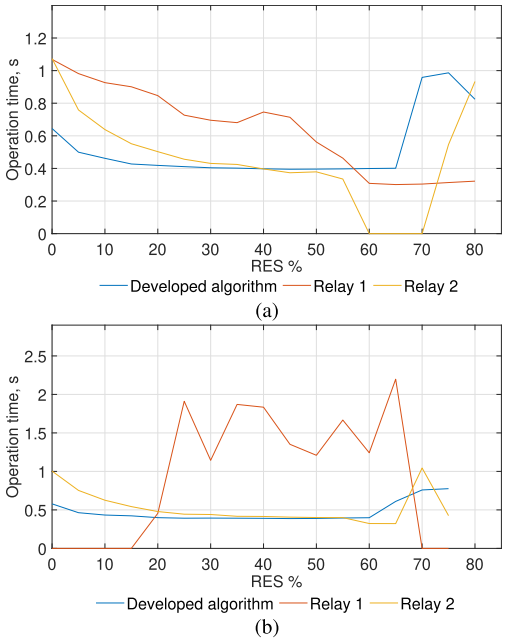

FIGURE 13. OOS protection operating times of protection devices for Case B. (a) represents a case study on the transmission line between buses 26-28 and (b) represents a case study on the transmission line between buses 28-29.

and Relay 2 respectively. For the transmission line between buses 16-17 both of the impedance-based protection relays failed to operate in the 55 % RES scenario and Relay 1 also failed to operate in the 60 % RES scenario, however, the developed algorithm successfully operated.

2) COMPARISON OF RESULTS IN CASE B

The protection operating time comparison for Case B is shown in Fig. 13. Overall, the developed algorithm has the same operating time in this simulation case compared to Relay 2. Compared to Relay 1, the developed algorithm operates 300 ms faster. Fig. 13a shows the operating times of the case study on the transmission line between buses 26-29, and Fig. 13b shows the protection operation times for the case study performed between buses 28-29. It can be observed that compared to simulation Case A the protection operation times are closer together for this case. The developed protection algorithm displays very similar operating times to Relay 2, whilst Relay 1 shows slower operating times for the majority of conducted tests. For the cases performed on the transmission line between buses 26-28, it should be noted that Relay 1 issued a trip command from the distance protection function instead of the OOS protection function. This applies to tests conducted with 60 % and above RES % scenarios. Additionally, it can be seen that Relay 2 does not operate for some of the RES % scenarios, whilst the other two tested devices do.

Regarding the case study performed on the transmission line between buses 28-29, it can be seen that in this case Relay 1 fails to operate on lower RES % as well as higher.

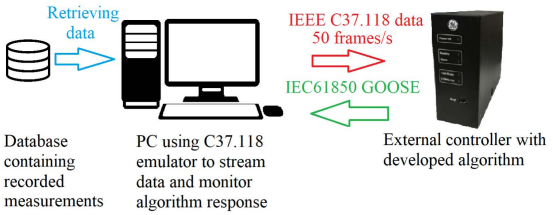

FIGURE 14. Developed protection algorithm testing setup with measured data streaming.

In addition, the operating time is higher compared to the other two tested approaches, because in this case study the protection operates on the second swing.

B. PROTECTION TESTING RESULTS USING OUT-OF-STEP EVENT RECORDINGS

The developed OOS protection algorithm has been also tested using event recordings from the Icelandic power system. To test the algorithm, the recorded historical PMU data has been streamed from a personal computer (PC) using a C37.118 emulator. The data was streamed to the phasor-based controller, where the developed algorithm is installed. The experimental setup for this case is shown in Fig. 14. The response of the algorithm has been recorded for a total of four OOS events that have been studied. The developed solution showed good results, providing successful operation for all of the recorded OOS events. The OOS event recordings used for the algorithm testing are described as follows:

- Event 1 and event 2 are nearly identical; both events were initiated by a flashover at a substation in the northern corridor of the power system, followed by its disconnection; the increased power flow through the southern corridor triggered an OOS event in the power system.
- Event 3 was initiated by an energization of a transmission line in the eastern part of the system, which caused undamped oscillations between the two centers of inertia, however, the OOS condition did not occur on the protected line.
- Event 4 was initiated by a large loss of load in the south-western part of the network. After this contingency, overload protection operated on the northern part of the ring connection, and an inter-trip separated the two generators in the southern corridor, which, after a few oscillations, resulted in an OOS condition on the southern ring connection.

Figs. 15 and 16 show the developed protection algorithm response, the voltage variations at the two measurement locations on the southern link and the measured power for Event 1 and Event 2, respectively. For both events the power system first goes through a stable swing and afterwards becomes unstable, resulting in an OOS situation. The dashed line denoted by ① shows the start of the event. From the protection signals shown in Figs. 15a and 16a for Event 1 and Event 2 respectively, it can be observed that during the ifirst

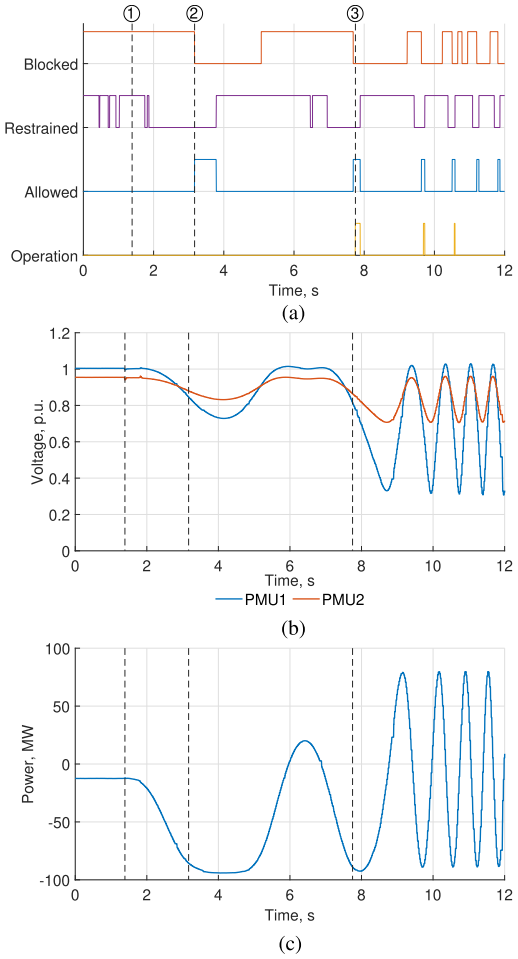

FIGURE 15. Protection algorithm response to Event 1 data. The dashed line marked as ① shows the start of the OOS event at 1.3 seconds. (a) the protection algorithm signals from the controller, (b) the voltage at the two measurement locations in the southern corridor and (c) the measured power in the southern corridor during the event.

stable swing the protection algorithm performs correctly. During this process the algorithm gets deblocked, indicated by ②, due to the occurred voltage dips in the system, and subsequently the restraint criteria are also lifted. The protection, however, does not give a trip signal, because the swing is stable. The second power swing becomes unstable for both events due to the large oscillations in voltages and power. For the unstable swings, the developed protection operates correctly, which can be seen from the operation signal traces indicated by ③. Since there is no specific OOS protection currently active in the Icelandic system, the recorded event continuous to evolve into OOS oscillations with increasing frequency, until a distance protection operates somewhere in the network. As shown in Figs. 15 and 16, this situation could have been resolved more rapidly using the proposed OOS solution.

Fig. 17 shows the developed protection algorithm response, the measured voltages at the two ends of the southern corridor, and the corridor power for OOS Event 3. From this

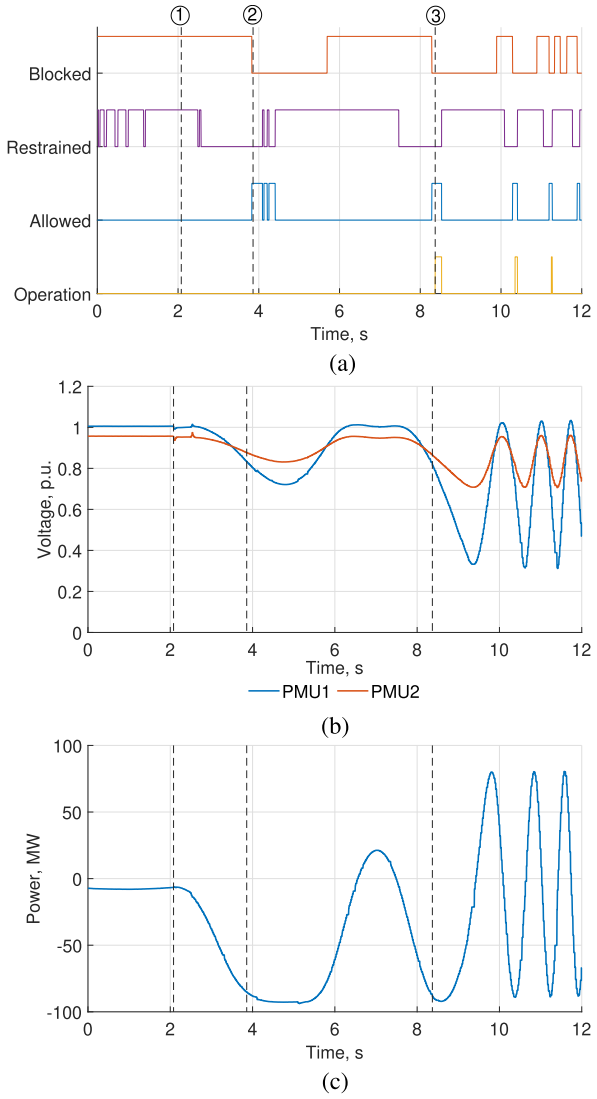

FIGURE 16. Protection algorithm response to Event 2 data. The dashed line marked as ① shows the start of the OOS event at 2.1 seconds. (a) the protection algorithm signals from the controller, (b) the voltage at the two measurement locations in the southern corridor and (c) the measured power in the southern corridor during the event.

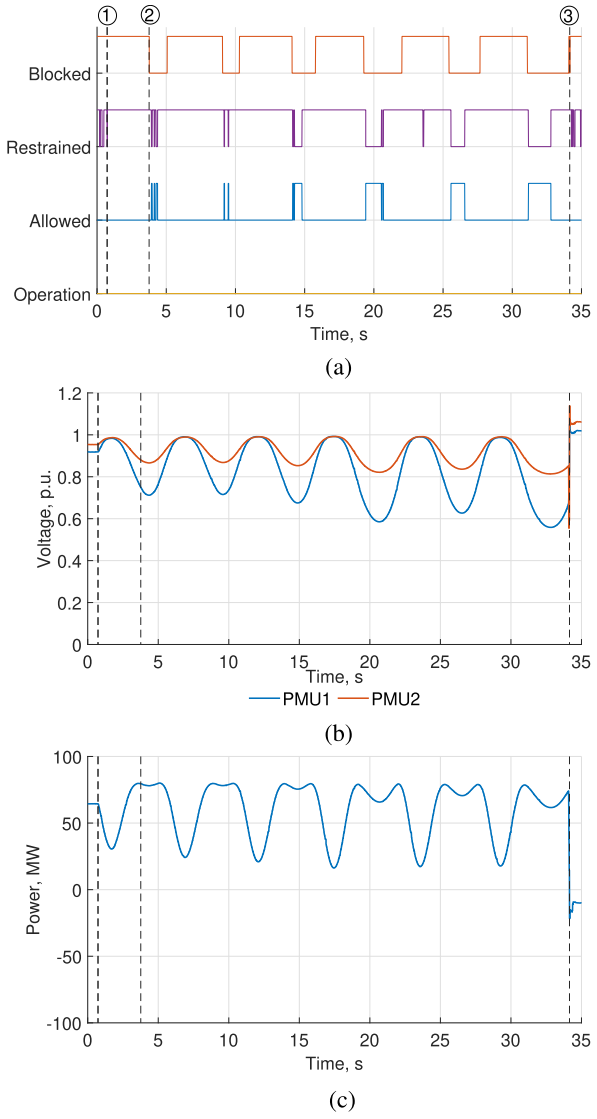

FIGURE 17. Protection algorithm response to Event 3 data. The dashed line marked as ① shows the start of the OOS event at 0.5 seconds. (a) the protection algorithm signals from the controller, (b) the voltage at the two measurement locations in the southern corridor and (c) the measured power in the southern corridor during the event.

figure it can be observed that after the line energization at 0.5 seconds, marked by ①, the system starts to oscillate. The oscillations are undamped and increasing in magnitude for both voltages and measured power, as can be seen in Figs. 17b and 17c. From the protection signal response shown in Fig. 17a, it can be seen that the protection algorithm is deblocked during the power swings, first of which is denoted by ②. As the OOS condition does not show on the protected line, the protection is stable and does not provide any operation command. The condition is cleared by a distance protection operation elsewhere in the network, indicated by ③ at 34 seconds. Therefore, it can be concluded that the developed protection algorithm is stable when the OOS condition is not localized to the protected tie-line.

Fig. 18 shows the developed algorithm response, measured voltages at the two locations in the southern link and the power flow for OOS Event 4. The dashed line marked in the figure shows the start of the event with the loss of load at 1.3 seconds, indicated by ①. Following the initial loss of load, it can be seen that the power transfer through the corridor, shown in Fig. 18c, starts increasing. At the same time, the voltages, shown in Fig. 18b, decrease, which leads to disabling the blocking criterion of the algorithm, as can be seen from the protection signals shown in Fig. 18a. At the time of 1.8 seconds a jump in power transfer occurs, marked by ②. This signifies the northern corridor disconnection due to overload. Thereafter, the southern ring connection experiences four stable swings, with progressively increasing

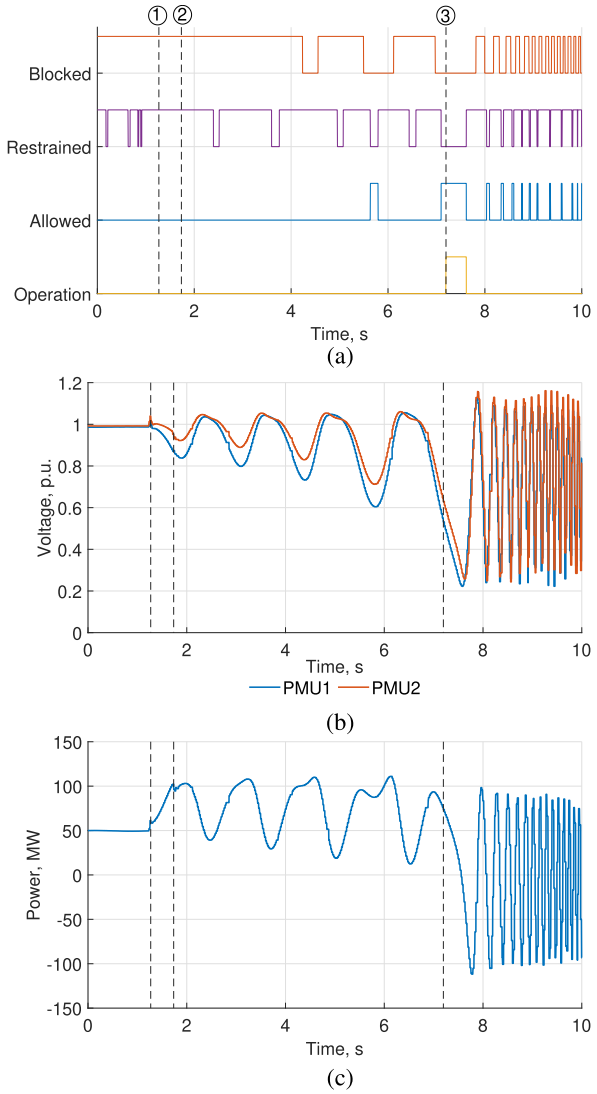

FIGURE 18. Protection algorithm response to Event 2 data. The dashed line marked as ① shows the start of the OOS event at 1.3 seconds. (a) the protection algorithm signals from the controller, (b) the voltage at the two measurement locations in the southern corridor and (c) the measured power in the southern corridor during the event.

magnitude, during which the protection does not operate. After the fourth swing, the system runs into instability, and the protection operates (marked as ③) due to the OOS conditions being fulfilled.

C. PROTECTION TESTING RESULTS FROM ICELANDIC POWER SYSTEM SIMULATIONS

Using the previously verified Icelandic power system model, which was developed in Section IV for real-time simulation, a number of tests were carried out. The simulations were conducted using Event 1 and Event 4 pre-fault conditions as the base case. Different grid conditions were used to test the developed protection algorithm. This was done by switching the series capacitor on the southern link in and out of operation, as well as disconnecting lines in the system. The simulations consisted of symmetrical and asymmetrical faults performed on different transmission lines in the network including single-pole reclose. From the numerous simulation results, it can be concluded that:

- The algorithm is stable when the power system experiences damped oscillations.
- The algorithm does not operate during single pole tripping and reclosing process.
- The algorithm provides operation for cases when an OOS event occurs for both the southern ring connection and the northern ring connection.

Based on the conducted tests, it can be concluded that the algorithm offers high security and dependability for OOS protection in the power network.

VI. CONCLUSION

In this paper a new OOS protection algorithm based on discrete angle derivatives has been presented, which is tested and implemented on hardware. The testing of the developed algorithm is done by using real-time simulations that build on the well-studied IEEE 39 bus power network. The performance of the developed algorithm is compared to the conventional impedance-based OOS protection relays. Furthermore, the algorithm is tested using the developed and validated real-time simulations model of the Icelandic transmission network, as well as using recorded data from several OOS events that occurred in the Icelandic power system. The algorithm shows reliable and fast operation for various states of the grid in the case of OOS events, and high security during stable power swings. The developed algorithm is fully measurement-based and settingless. Therefore, it is suitable to be applied on arbitrary locations in power systems, where OOS conditions are expected to occur. The results of the simulations and numerous tests show that:

- The developed algorithm performs better in terms of operating time compared to present commercially available impedance-based protection devices.
- Based on the case studies, the algorithm has higher reliability than the impedance-based protection algorithms.
- In addition to numerical real-time simulations, the algorithm has been also tested on actual recordings of OOS events, which proves its stability and dependability for real installations.

Finally, the concept has been tested and implemented in practice by Landsnet in their WACS scheme.

ACKNOWLEDGMENT

The financial support provided by the Dutch Scientific Council NWO is highly appreciated. The first author thanks Delft University of Technology for providing the opportunity to conduct this research work at TU Delft. The cooperation and support provided by Landsnet hf. and GE Renewable Energy is highly acknowledged.

REFERENCES

[1] J. Blumschein, Y. Yelgin, and M. Kereit, "Blackout prevention by power swing detection and out-of-step protection," *J. Power Energy Eng.*, vol. 2, no. 4, pp. 694–703, 2014.

[2] D. A. Tziouvaras and D. Hou, "Out-of-step protection fundamentals and advancements," in *Proc. 57th Annu. Conf. Protective Relay Eng.*, 2004, pp. 282–307.
[3] A. Sauhats, A. Utans, and E. Biela-Dalidovicha, "Equal area criterion and angle control-based out-of-step protection," in *Proc. IEEE 58th Int. Scientific Conf. Power Electr. Eng. Riga Tech. Univ. (RTUCON)*, Oct. 2017, pp. 1–6.
[4] C. W. Taylor, J. M. Haner, L. A. Hill, W. A. Mittelstadt, and R. L. Cresap, "A new out-of-step relay with rate of change of apparent resistance augmentation," *IEEE Trans. Power App. Syst.*, vol. PAS-102, no. 3, pp. 631–639, Mar. 1983.
[5] *MiCOM O40 Agile P543/P545 Technical Manual Ver92M*, Schneider Electric, Rueil-Malmaison, France, 2021.
[6] S. Paudyal, R. Gokaraju, M. S. Sachdev, and S. Cheng, "Out-of-step detection using energy equilibrium criterion in time domain," *Electr. Power Compon. Syst.*, vol. 37, no. 7, pp. 714–739, Jun. 2009.
[7] S. Paudyal, G. Ramakrishna, and M. S. Sachdev, "Application of equal area criterion conditions in the time domain for out-of-step protection," *IEEE Trans. Power Del.*, vol. 25, no. 2, pp. 600–609, Apr. 2010.
[8] M. Abedini, M. Davarpanah, M. Sanaye-Pasand, S. M. Hashemi, and R. Iravani, "Generator out-of-step prediction based on faster-than-real-time analysis: Concepts and applications," *IEEE Trans. Power Syst.*, vol. 33, no. 4, pp. 4563–4573, Jul. 2018.
[9] K. Sreenivasachar, "Out-of-step detection on transmission lines using apparent impedance differential method," *IEEE Trans. Power Del.*, early access, Nov. 8, 2021, doi: 10.1109/TPWRD.2021.3125525.
[10] P. Regulski, W. Rebizant, M. Kereit, and H.-J. Herrmann, "PMU-based generator out-of-step protection," *IFAC-PapersOnLine*, vol. 51, no. 28, pp. 79–84, 2018.
[11] T. D. Duong, S. D'Arco, and A. Holdyk, "A method for predictive out-of-step tripping based on synchrophasors," in *Proc. 15th Int. Conf. Develop. Power Syst. Protection (DPSP)*, 2020, pp. 1–6.
[12] J. R. Camarillo-Penaranda, D. Celeita, M. Gutierrez, M. Toro, and G. Ramos, "An approach for out-of-step protection based on swing center voltage estimation and analytic geometry parameters," *IEEE Trans. Ind. Appl.*, vol. 56, no. 3, pp. 2402–2408, May 2020.
[13] N. G. Chothani, B. R. Bhalja, and U. B. Parikh, "New support vector machine-based digital relaying scheme for discrimination between power swing and fault," *IET Gener., Transmiss. Distrib.*, vol. 8, no. 1, pp. 17–25, Jan. 2014.
[14] M. R. Aghamohammadi and M. Abedi, "DT based intelligent predictor for out of step condition of generator by using PMU data," *Int. J. Electr. Power Energy Syst.*, vol. 99, pp. 95–106, Jul. 2018. [Online]. Available: https://www.sciencedirect.com/science/article/pii/S0142061517321397
[15] E. A. Frimpong, P. Y. Okyere, and J. Asumadu, "On-line determination of transient stability status using MLPNN," in *Proc. IEEE PES PowerAfrica*, Jun. 2017, pp. 23–27.
[16] M. Tealane, J. Kilter, M. Popov, O. Bagleybter, and D. Klaar, "Online detection of out-of-step condition using PMU-determined system impedances," *IEEE Access*, vol. 10, pp. 14807–14818, 2022.
[17] D. Fan and V. Centeno, "Adaptive out-of-step protection schemes based on synchrophasors," in *Proc. IEEE PES Gen. Meeting | Conf. Expo.*, Jul. 2014, pp. 1–5.
[18] K. Shimizu and A. Ishigame, "Novel transient stability assessment using post-disturbance voltage fluctuations," in *Proc. Int. Conf. Smart Grids Energy Syst. (SGES)*, Nov. 2020, pp. 12–17.
[19] Y. Cui, R. G. Kavasseri, and S. M. Brahma, "Dynamic state estimation assisted out-of-step detection for generators using angular difference," *IEEE Trans. Power Del.*, vol. 32, no. 3, pp. 1441–1449, Jun. 2017.
[20] J. R. A. K. Yellajosula, Y. Wei, M. Grebla, S. Paudyal, and B. A. Mork, "Online detection of power swing using approximate stability boundaries," *IEEE Trans. Power Del.*, vol. 35, no. 3, pp. 1220–1229, Jun. 2020.
[21] S. Zhang and Y. Zhang, "A novel out-of-step splitting protection based on the wide area information," *IEEE Trans. Smart Grid*, vol. 8, no. 1, pp. 41–51, Jan. 2017.
[22] H. Zare, H. Yaghobi, and Y. Alinejad-Beromi, "Adaptive concept of controlled islanding in power systems for wide-area out-of-step prediction of synchronous generators based on adaptive tripping index," *IET Gener., Transmiss. Distrib.*, vol. 12, no. 16, pp. 3829–3836, Sep. 2018.
[23] M. R. Nasab and H. Yaghobi, "A real-time out-of-step protection strategy based on instantaneous active power deviation," *IEEE Trans. Power Del.*, vol. 36, no. 6, pp. 3590–3600, Dec. 2021.
[24] J. P. Desai and V. H. Makwana, "Phasor measurement unit incorporated adaptive out-of-step protection of synchronous generator," *J. Modern Power Syst. Clean Energy*, vol. 9, no. 5, pp. 1032–1042, 2021.
[25] B. Deshmukh, S. Biswal, and D. K. Lal, "Synchronous generator out-of-step protection based on Savitzky–Golay filtering technique," in *Proc. Emerg. Trends Ind. 4.0 (ETI)*, May 2021, pp. 1–3.
[26] E. Farantatos, R. Huang, G. J. Cokkinides, and A. P. Meliopoulos, "A predictive generator out-of-step protection and transient stability monitoring scheme enabled by a distributed dynamic state estimator," *IEEE Trans. Power Del.*, vol. 31, no. 4, pp. 1826–1835, Aug. 2016.
[27] P. Kundur, *Power System Stability and Control*. New York, NY, USA: McGraw-Hill, 1994.
[28] Y. Xue, T. Van Custem, and M. Ribbens-Pavella, "Extended equal area criterion justifications, generalizations, applications," *IEEE Trans. Power Syst.*, vol. 4, no. 1, pp. 44–52, Feb. 1989.
[29] M. Pavella, E. Damien, and D. Ruiz-Vega, *Transient Stability of Power Systems*. Cham, Switzerland: Springer, 2000.
[30] M. Meldorf and J. Kilter, *Elektrisüsteemi Stabiilsus*. Tallinna, Estonia: Tehnikaülikooli Kirjastus, 2011.
[31] J. Machowski, Z. Lubosny, J. W. Bialek, and J. R. Bumby, *Power System Dynamics: Stability and Control*, 3rd ed. Hoboken, NJ, USA: Wiley, 2020.
[32] GE Digital. (2021). *Phasor Controller*. [Online]. Available: https://www.ge.com/digital/applications/transmission/phasorcontroller
[33] *IEEE Standard for Phasor Data Concentrators for Power Systems*, Standard C37.247, 2019.
[34] *Modelling of Permanent Magnet Generator Based Wind Turbine Systems in the RTDS*, RTDS Technologies, Winnipeg, MB, Canada, 2017.
[35] *SIPROTEC 4 Line Differential Protection with Distance Protection 7SD5 V4.7*, Siemens AG, Munich, Germany, 2016.
[36] *Easergy MiCOM P44y Technical Manual*, Schneider Electric, Rueil-Malmaison, France, 2019.
[37] LandsNet. *LandsNet's Transmission System*. Accessed: Mar. 30, 2022. [Online]. Available: https://landsnet.is/

MARKO TEALANE (Student Member, IEEE) received the B.Sc. and M.Sc. degrees in electrical power engineering from the Tallinn University of Technology, in 2014 and 2016, respectively, where he is currently pursuing the Ph.D. degree in electrical power engineering. From 2019 to 2020, he was an Academic Visitor with the Delft University of Technology, where he was working on out-of-step protection in the Intelligent Electrical Power Grids Group. In the past, he worked as a Protection Engineer at the Estonian Transmission System Operator. He is currently on sabbatical leave, and works at TU Delft. His research interests include power system protection, power system relaying, and wide-area control.

JAKO KILTER (Senior Member, IEEE) received the B.Sc. and M.Sc. degrees in electrical power engineering from the Tallinn University of Technology, and the Ph.D. degree in electrical power engineering from the Tallinn University of Technology, in 2009. He is currently a Professor in power systems and the Head of the Power Systems Research Group, School of Engineering, Tallinn University of Technology, the Chairperson of the High Voltage Committee with the Estonian Centre for Standardization and Accreditation, and the Co-Chair of CIGRE Estonian National Committee. His research and consultancy work over the years has been split between the areas of power system dynamics, wide-area control and applications, and power quality.

OLEG BAGLEYBTER (Member, IEEE) received the Diploma degree in electrical engineering and the Ph.D. degree from Irkutsk Technical University, in 1999 and 2006, respectively. He is currently working as a Senior Staff Engineering Manager at GE. He is responsible for advanced automation applications research and development portfolio within the GE Grid Automation Business. His focus is on developing and deploying innovative applications and solutions utilizing wide area measurements in transmission and distribution grids. He has worked in the past as a Protection and Control Engineer for a power utility in Siberia and a Product Manager for transmission protection relays for GE Grid Solutions.

BIRKIR HEIMISSON received the B.Sc. degree in electrical engineering from the University of Iceland, in 2011, and the M.Sc. degree in electric power engineering from Chalmers University, in 2014. He joined Landsnet (TSO of Iceland) as a System Operator, in 2014. Together with system operation, he led the smart-grid development with focus on wide-area-measurements and control. Additionally, he was the work-package leader for Landsnet in EU Horizon 2020 MIGRATE Project. In 2019, he moved to research and development, where he focuses on digital substation implementation based on IEC 61850 and smart-grid development.

MARJAN POPOV (Fellow, IEEE) received the Ph.D. degree in electrical power engineering from the Delft University of Technology, Delft, in 2002. He is currently a Chevening Alumnus. In 1997, he was an Academic Visitor with the University of Liverpool, Liverpool, U.K., working in the Arc Research Group on modeling SF6 circuit breakers. His research interests include future power systems, large-scale power system transients, intelligent protection for future power systems, and wide-area monitoring and protection. He is a member of Cigre and actively participated in WG C4.502 and WG A2/C4.39. In 2010, he received the prestigious Dutch Hidde Nijland Prize for extraordinary research achievements. He was a recipient of the IEEE PES Prize Paper Award and IEEE Switchgear Committee Award in 2011 and an Associate Editor for Elsevier's International Journal of Electrical Power and Energy Systems. In 2017, together with the Dutch utilities TenneT, Alliander, and Stedin, he founded the Dutch Power System Protection Centre to promote the research and education in power system protection.